Crosslinker-Free Hyaluronic Acid Aerogels

Daniel Aguilera-Bulla, Laurianne Legay, Sytze Buwalda, Tatiana Budtova

Crosslinker-free hyaluronic acid aerogels

Daniel Aguilera-Bulla, Laurianne Legay, Sytze J. Buwalda*, Tatiana Budtova*

MINES Paris, PSL Research University, Center for Materials Forming (CEMEF), UMR CNRS 7635, CS 10207, 06904 Sophia Antipolis, France.

Corresponding authors:

Tatiana.Budtova@minesparis.psl.eu

Sijtze.Buwalda@minesparis.psl.eu

Abstract

Aerogels based on hyaluronic acid (HA) were prepared without any chemical crosslinking by polymer dissolution, network formation via non-solvent induced phase separation and supercritical CO_2 drying. The influence of solution pH, concentration of HA and type of non-solvent on network volume shrinkage, aerogel density, morphology and specific surface area was investigated. A marked dependence of aerogel properties on solution pH was observed: aerogels with the highest specific surface area, 510 m^2/g, and the lowest density, 0.057 g/cm^3, were obtained when the HA solution was at its isoelectric point (pH 2.5). This work reports the first results ever on neat HA aerogels and constitutes the background for their use as advanced materials for biomedical applications.

Keywords: Bio-aerogels, hyaluronic acid, porous materials, density, specific surface area, morphology

1. Introduction

Bio-aerogels are a unique class of dry, highly porous, nanostructured polysaccharide materials with low density and high internal surface area.[1-3] They can be prepared by removing the liquid from a polysaccharide gel using drying with supercritical (sc) CO_2. The latter avoids the development of capillary stresses and, theoretically, preserves network morphology. In hydrated form, bio-aerogels resemble bio-based hydrogels and, accordingly, display advantageous properties including biomimicry.[4] Furthermore, the specificities of preparing aerogels allow their properties and structure to be varied more widely. In addition, thanks to their dry nature, bio-aerogels keep their shape better than hydrogels during long-time storage and bacterial contamination is avoided. Bio-aerogels have been prepared in various shapes, including monoliths,[5, 6] millimeter-sized beads[7, 8] and microparticles.[9, 10] Thanks to their high porosity and low density, bio-aerogels generally have very low thermal conductivity and have been proposed as thermal insulation materials.[11] Bio-aerogels have also found application as food packaging,[12] catalyst support[13] and absorption/adsorption material.[14] In the last decade, bio-aerogels have attracted increasing interest as biomaterials thanks to their unique properties.[15, 16] For example, our group recently prepared pectin and pectin-cellulose aerogels for pH-controlled release of theophylline.[17-19]

Among the various polysaccharides, HA is an especially promising candidate regarding the preparation of aerogels for biomedical applications. HA, a linear anionic polysaccharide, is part of the natural extracellular matrix and exhibits important functional and structural roles in the body. HA plays a significant role in tissue regeneration and promotes dermal regeneration. Because of these properties, HA has been used extensively for biomedical applications such as regenerative medicine and controlled drug delivery, which has been the topic of several reviews.[20-22] Various

types of HA based biomaterials have been described in the literature, including hydrogels[23], cryogels[24], sponges[25] and films.[26]

It is known that materials made from neat HA possess poor mechanical properties, in particular, in hydrated state. Various "reinforcing" strategies have been applied: HA chemical crosslinking, HA functionalization followed by crosslinking, non-covalent "auto-crosslinking" (H-bonding between carboxylate and acetamido groups or hydrophobic interactions), and mixing with other polymers. In the latter case, often solutions of gelling polymers are used and/or HA is crosslinked with or grafted on the second component (see, for example [21, 27]). Carboxyl and hydroxyl groups in HA can be used for crosslinking via ester and ether groups, respectively. For example, chemical crosslinking with another polymer, poly(methyl vinyl ether-*alt*-maleic anhydride), was performed under heating; ester groups were formed and sponges were prepared via freeze-drying.[25] Another example was reported in [24]: HA was methacrylated and *N*, *N*-dimethylacrylamide was used as a crosslinker; cryogels were obtained under freeze-drying. Various ways of HA network formation for making porous materials have been discussed in [21, 22].

Till now, only one approach has been used to make HA-based aerogels: HA was mixed with alginate followed by alginate crosslinking with calcium ions.[28, 29] Micro-particles with an average diameter of 5 μm were obtained via an emulsion-gelation method. The authors stated the absence of interactions between HA and calcium ions, and mentioned the potential formation of hydrogen bonds between the carboxylate groups of alginate and the amide groups of the N-acetyl-D-glucosamine of HA. The incorporation of HA helped to reduce agglomeration of the particles, which was ascribed to increased particle surface charge and hence increased repulsion between particles. These microparticles were suggested as potential drug carriers for pulmonary administration[28]; the kinetics of naproxen release were investigated in [29].

We hypothesize that it is also possible to make aerogels using HA alone and without crosslinking. Aerogels based on neat HA have never been reported, which offers the scientific challenge of establishing processing-structure-properties relationships. The goal of the current work was i) to evaluate which conditions lead to the formation of HA "aerogels", i.e. materials with low density and high specific surface area, and b) to characterize these aerogels. No crosslinking was used; the network was formed via non-solvent induced phase separation and dried with sc drying CO_2. The influence of solution pH, HA concentration and type of non-solvent on volume shrinkage, density, specific surface area and morphology of the dry materials was investigated.

2. Experimental

2.1. Materials

Hyaluronic acid in the form of sodium hyaluronate was purchased from Acros Organics (95% purity, molecular weight 1.5 to $2.2 \cdot 10^6$ g/mol as given by the manufacturer); the exact molecular weight was determined with viscometry and is presented in the Results and Discussion section. Absolute ethanol (EtOH), sodium hydroxide (NaOH) and hydrochloric acid (HCl, 32%) were purchased from Fisher Scientific. All products were used as received. Water was distilled.

2.2. Methods

2.2.1. Preparation of HA dry materials

HA powder was dissolved in water at 0.5 or 1.6 wt% under mechanical stirring. The desired pH value of the HA solution was achieved via drop-wise addition of 1 M HCl or 1 M NaOH solution. Then, HA solutions (13 g) of different pH were poured in cylindrical molds of 27.5 mm in diameter and centrifuged twice for 45 min at 4500 rpm to eliminate bubbles.

The methodology employed for the preparation of HA aerogel precursors using non-solvent induced phase separation was based on a previously reported procedure for bio-aerogels.[17, 30, 31] Briefly, non-solvent (acetone or ethanol) was slowly added to the HA solutions in order to induce coagulation and the formation of a HA network. The proportion of HA solution/non-solvent was kept at 1:2 in volume. After 48 h, the non-solvent was removed and replaced by fresh one. The procedure was repeated six times to achieve complete replacement of water by ethanol or acetone, both of which are fully miscible with sc CO_2 (Figure 1). These samples will be called "precursors".

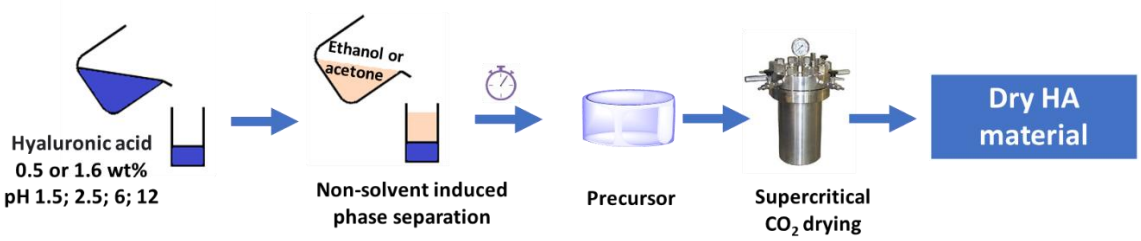

Figure 1. Schematic representation of the protocol of HA-based materials' preparation using the non-solvent induce phase separation methodology.

The protocol to obtain dry materials from the HA precursors using sc CO_2 drying was based on a previously reported method.[17, 30-32] The precursors were placed in a 1 L autoclave with an excess of ethanol or acetone, depending on the non-solvent used. The system was pressurized at 50 bar and 37 °C in order to purge progressively the non-solvent. Then, the pressure was increased to 80 bar at constant temperature (37 °C) to reach sc CO_2 conditions. The system was kept at these conditions during 1 h with an output of 5 kg of CO_2/h to perform a dynamic wash and remove the remaining non-solvent from the precursor. After this cycle, the system was left in a static mode for 1-2 h and another dynamic cycle of washing of 2 h was launched to assure complete removal of the non-solvent. The depressurization was carried out with a ramp of 4 bar/h at 37 °C. After reaching room temperature the autoclave was opened and the materials were collected.

As it will be shown in the following, not all dry HA materials resulted in "aerogels", i.e. materials with low density (below 0.2 g/cm^3) and high specific surface area (at least 100 m^2/g).[33] We will use "dry HA material" as a general term and "aerogel" when the material fits the above definition.

2.2.2. Characterization

The molecular weight of the native HA and of HA in selected aerogel samples was determined from the intrinsic viscosity using the Mark-Houwink equation using 0.1 M of NaCl as solvent at 25 °C:

$$[\eta] = K \times M^a \quad (1)$$

with K = 3.36·10^{-4} dL/g and a = 0.79.[34]

The Hansen solubility parameter (δ) of HA was calculated as follows[35]:

$$\delta = ({\delta_d}^2 + {\delta_p}^2 + {\delta_h}^2)^{1/2} \quad (2)$$

where δ_d, δ_p and δ_h are the dispersion, polar and hydrogen bonding solubility parameters, respectively (values are taken from[36] and given in Table S1).

The difference in solubility parameters (Δδ) for each pair (HA-acetone and HA-ethanol) was calculated as follows[35]:

$$\Delta\delta = [4(\delta_{d,P} - \delta_{d,S})^2 + (\delta_{p,P} - \delta_{p,S})^2 + (\delta_{h,P} - \delta_{h,S})^2]^{1/2} \quad (3)$$

where "P" corresponds to "polymer" (here, HA) and "S" corresponds to "solvent" (here, acetone or ethanol). The dispersion, polar and hydrogen bonding parameters of ethanol and acetone are known[35] and also provided in Table S1.

The percentages of volume shrinkage during solvent exchange (ΔV_{ex}) and total shrinkage (ΔV_{total}) were determined by equation 4 and 5, respectively:

$$\Delta V_{ex}(\%) = \left(\frac{V_{ini} - V_{pr}}{V_{ini}}\right) \times 100 \quad (4)$$

$$\Delta V_{total}(\%) = \left(\frac{V_{ini} - V_{final}}{V_{ini}}\right) \times 100 \quad (5)$$

where V_{ini}, V_{pr} and V_{final} are the volumes of the initial HA solution, of the precursor and of the dry material, respectively.

The bulk density (ρ_{bulk}) of the materials was calculated by determining their mass and volume (measured with a digital balance and a digital caliper, respectively). The skeletal density (ρ_{sk}) was measured via helium pycnometry (MPY-2, Quantachrome, Boynton Beach, FL, USA) at room temperature and atmospheric pressure. The values of shrinkage and densities were obtained by averaging three to six measurements.

The porosity (ε) and the total pore volume (V_p) were calculated using equations 6 and 7, respectively:

$$\varepsilon = \left(1 - \frac{\rho_{bulk}}{\rho_{sk}}\right) \times 100 \quad (6)$$

$$V_p = \left(\frac{1}{\rho_{bulk}} - \frac{1}{\rho_{sk}}\right) \quad (7)$$

The specific surface area (S_{BET}) was evaluated by nitrogen adsorption using an ASAP 2020 instrument (Micromeritics) applying the Brunauer–Emmett–Teller (BET) method. Before the analysis, the HA dry samples were degassed at 70 °C for 10 h.

Morphological characterization was performed by scanning electron microscopy (SEM) using a Zeiss Supra 40 microscope equipped with a field emission gun. Prior to analysis, HA-materials were sputter-coated with a double platinum layer of 7 nm using a Q150T Quarum metallizer.

Image analysis of SEM micrographs for pore size distribution was carried out using ImageJ software (1.53k, Rayne Rasband, National Institutes of Health, USA; http://rsb.info.nih.gov/ij/). Aerogels prepared at pH 2.5 were selected and their SEM images with a magnification of 200kx were analyzed. The image was first sharpened, and pores' circularity from 0.15 to 1 was set as a compromise between an adequate representation of the pores and elimination of "defects". The

areas below 10 pixels were discarded. From 450 to 750 pores per formulation were analyzed. Pore size distribution analysis was performed using GraphPad Prism v. 9.0.2 (GraphPad Software, La Jolla, CA, USA) by variance analysis applying one way ANOVA and Tuckey's test with a level of significance (α) of 0.05.

3. Results and Discussion

The intrinsic viscosity of HA was determined as described in Methods[34] and found to be 21.32 dL/g. The molecular weight was estimated to be around $1.2 \cdot 10^6$ g/mol, which is slightly lower than the molecular weight indicated by the manufacturer, $1.5\text{-}2.2 \cdot 10^6$ g/mol.

Table 1 gives an overview of the formulations that were evaluated for the preparation of HA dry materials. Two concentrations of hyaluronic acid were assessed (0.5 and 1.6 wt%), four pH values of the initial HA solution were used (pH=1.5, 2.5, 6.0 and 12) and the coagulation of HA was carried out using either ethanol (E) or acetone (A) as non-solvent, resulting in 16 different preparation conditions.

Table 1. Overview of the formulations evaluated for the preparation of HA dry materials. Sample label summarizes the parameters of sample preparation: HA - hyaluronic acid, A - acetone, E - ethanol, the first number indicates HA concentration in solution and the second number solution pH.

Entry	Label	Non-solvent	HA concentration (wt%)	pH	Observation: self-standing precursor (Y/N)
1	HA-E-0.5-1.5	Ethanol	0.5	1.5	Yes
2	HA-E-0.5-2.5			2.5	Yes
3	HA-E-0.5-6.0			6	No

4	HA-E-0.5-12			12	Yes
5	HA-E-1.6-1.5		1.6	1.5	Yes
6	HA-E-1.6-2.5			2.5	Yes
7	HA-E-1.6-6.0			6	No
8	HA-E-1.6-12			12	Yes
9	HA-A-0.5-1.5	Acetone	0.5	1.5	Yes
10	HA-A-0.5-2.5			2.5	Yes
11	HA-A-0.5-6.0			6	No
12	HA-A-0.5-12			12	Yes
13	HA-A-1.6-1.5		1.6	1.5	Yes
14	HA-A-1.6-2.5			2.5	Yes
15	HA-A-1.6-6.0			6	Yes
16	HA-A-1.6-12			12	Yes

3.1. Shape stability of the HA precursors and appearance of the dried materials

As shown in Table 1, using ethanol as a non-solvent for HA solutions of 0.5 wt% (Table 1, entries 1-4) and 1.6 wt% (Table 1, entries 5-8) led to self-standing precursors at pH values of 1.5, 2.5 and 12; at pH 6 the precursors were falling apart and therefore not dried. In the cases where acetone was the non-solvent for 0.5 wt% HA solutions (entries 9-12) a similar trend was observed, with stable precursors formed at pH 1.5, 2.5 and 12. However, when acetone was added to 1.6 wt% HA solutions (entries 13-16), self-standing precursors were obtained at all the pH values assessed.

Summarizing, the non-solvent induced phase separation approach allowed obtaining 13 self-standing precursors from the 16 formulations evaluated. The self-standing precursors were subsequently dried with sc CO_2, and in all cases solid materials were obtained with different shapes

and brittleness (Figures 2 and S1). For example, samples prepared from 1.6 wt% HA solution coagulated in acetone (Figure 2) are mechanically very different depending on the pH value of the HA solution: the dry material obtained using pH 6 was highly friable while the one made using pH 2.5 did not crumble under manipulations and remained stable. Figures 2 and S1 show that samples prepared at pH 2.5 of other HA concentrations also kept their shape better compared to other pH values.

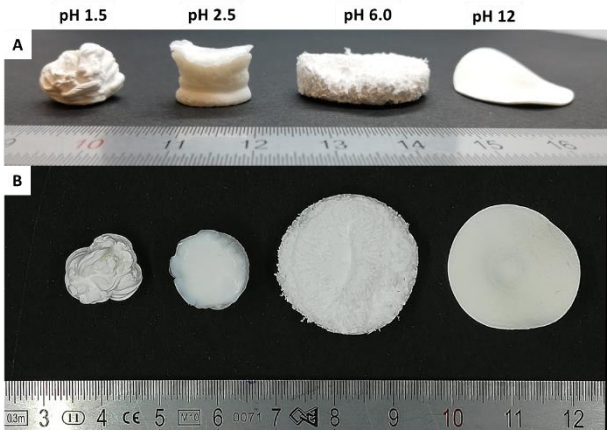

Figure 2

Examples of the side view (A) and top view (B) of HA dry materials obtained from 1.6 wt% HA solutions at pH 1.5, 2.5, 6 and 12, coagulated in acetone (entries 13-16 from Table 1).

3.2. Volume shrinkage

It is well known from the literature that solvent to non-solvent exchange and subsequent sc drying induce volume shrinkage of the sample.[30, 31, 37, 38] Shrinkage of a polymer from a coil swollen in a solvent to a globule in a non-solvent have been reported for numerous synthetic polymer solutions and gels. This is less studied for polysaccharide macromolecules that are semi-rigid: above the overlap concentration and upon the addition of a non-solvent, polysaccharides are

not collapsing but shrink to a different extent (depending on the polymer and non-solvent) forming a 3D network "filled" with a non-solvent (called precursor in Figure 1). The photos of sample volume evolution from 1.6 wt% HA solution at pH 2.5 to the precursor (here, non-solvent was acetone) and to the dry material are shown in Figure S2 as an example.

Volume shrinkage during solvent exchange (eq.4) and total shrinkage (eq.5) was evaluated as a function of solution pH, HA concentration and type of non-solvent (Figure 3). In all cases, shrinkage is very high, and it occurs mostly during solvent exchange.

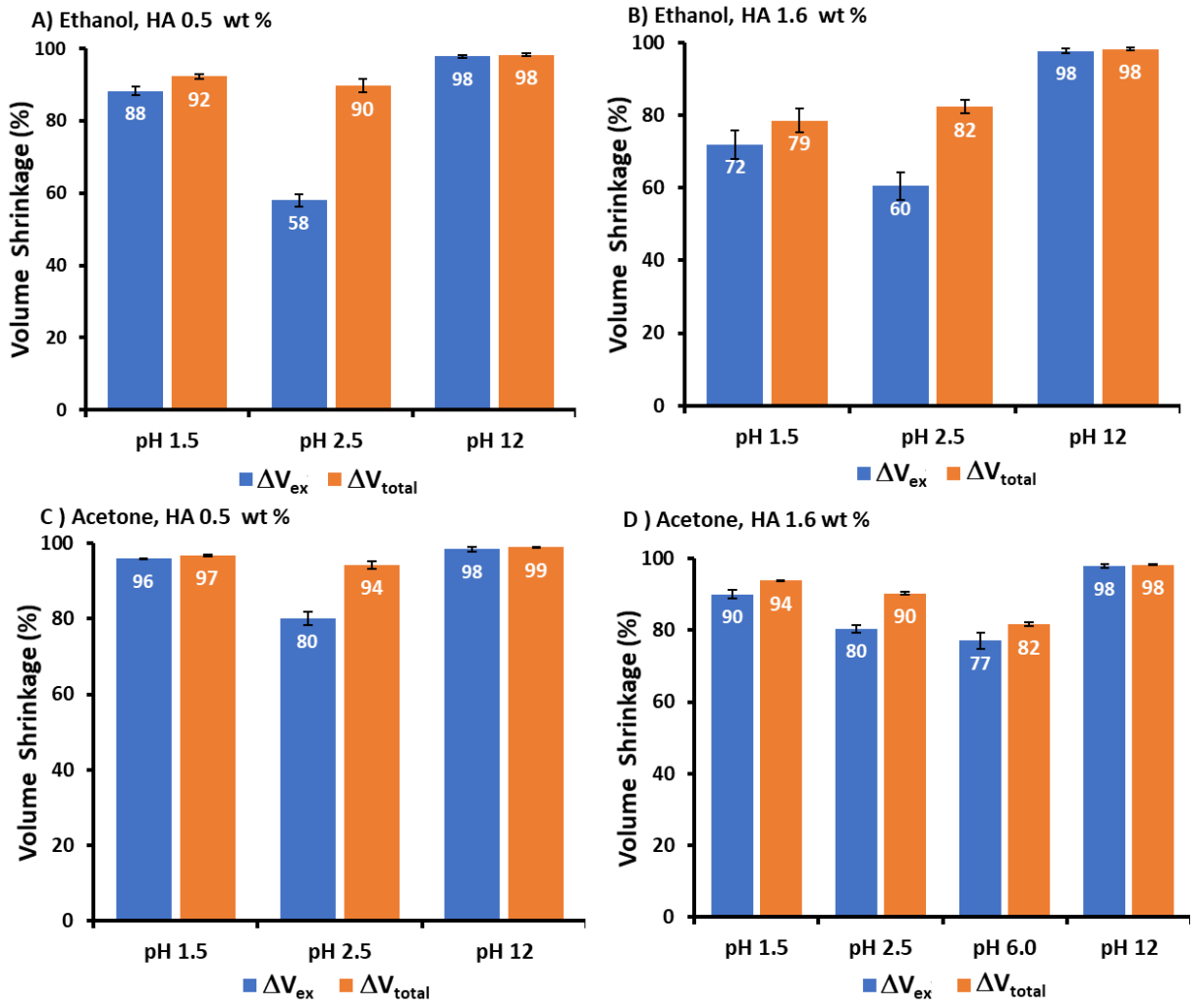

Figure 3

Volume shrinkage as a function of the type of non-solvent, pH and the concentration of HA. A) and B): ethanol as non-solvent, HA solutions of 0.5 and 1.6 wt% of HA, respectively. C) and D): acetone as non-solvent, HA solutions of 0.5 and 1.6 wt% of HA, respectively.

Figure 3 shows that whatever the non-solvent, shrinkage is higher for lower HA concentrations, which is a phenomenon that was also reported for other bio-aerogels.[30, 31, 37] It is supposed that a higher polymer concentration makes the network stronger and thus more "resistant" to non-solvent which induces chain contraction.

The use of a less polar solvent, such as acetone, leads to a higher shrinkage in comparison with ethanol for all the formulations studied (Figures 3). The reason is the higher affinity of HA towards ethanol as compared to acetone, which follows from the solubility parameters of HA, ethanol and acetone: 35.8, 26.5 and 19.9 $MPa^{1/2}$, respectively, see eq.2, Table S1 and reference [35]. The difference in solubility parameters for each pair was calculated with eq. 3: for the HA-ethanol (25.3 $MPa^{1/2}$) it is smaller in comparison with the HA-acetone (35.8 $MPa^{1/2}$). The same trend was reported for cellulose coagulated in different non-solvents[39]. When the concentration of HA was increased from 0.5 to 1.6 wt%, it was possible to obtain solid dry materials by coagulating in acetone from solutions of all pH values used, pH 6 being the value at which the least shrinkage occurred (Figure 2 and Figure 3D).

3.3. Bulk and skeletal density, porosity and pores' volume

As expected from the results obtained on samples' shrinkage, the preparation conditions (pH value of the initial HA solution, type of non-solvent and HA concentration) have a pronounced influence on the bulk density of dry materials (Figure 4). For example, depending on the pH of the

solution, in the case of ethanol as non-solvent (Figure 4A), the density varies from 0.057 g/cm^3 to 0.270 g/cm^3 for materials prepared from 0.5 wt% HA solution (blue bars), and from 0.065 g/cm^3 to 0.722 g/cm^3 for materials prepared from 1.6 wt% HA solutions (orange bars). In the case of acetone as non-solvent (Figure 4B), the density varies from 0.112 g/cm^3 to 0.574 g/cm^3 for materials from HA solutions of 0.5 wt%, and from 0.081 g/cm^3 to 0.952 g/cm^3 for materials from HA solutions of 1.6 wt%. The use of acetone resulted in denser materials in comparison with the materials prepared by coagulating in ethanol, as expected from the values of shrinkage. In general, a higher material density was observed for higher values of solution pH and a higher polymer concentration. For the latter, the higher polymer concentration is dominating the lower volume shrinkage resulting in a higher density, which agrees with previous reports on other bio-based aerogels.[30, 32, 37, 40-43]

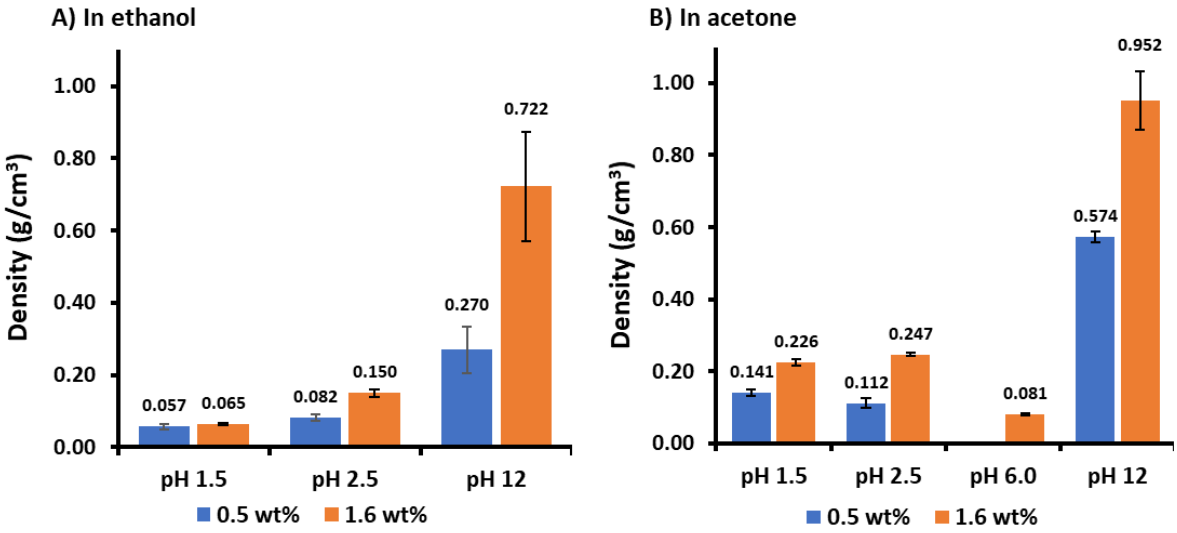

Figure 4

Bulk density of various HA dry materials obtained by coagulation in ethanol (A) and in acetone (B).

The skeletal density of the initial HA and of dry HA materials was determined by helium pycnometry. For the samples coagulated in ethanol it was 1.296 ± 0.009 and for the samples

coagulated in acetone 1.388 ± 0.063, similar to the skeletal density of the neat HA, 1.392 ± 0.028 g/cm^3.

The overall porosity (ε) and total pore volume (V_p) were calculated using equations 6 and 7, respectively (Table 2). As expected from the values of the bulk density (Figure 4), porosity and pore volume are the lowest for sample HA-A-1.6-12; the highest values were obtained for HA-E-0.5-1.5 and HA-E-1.6-1.5.

Table 2. Bulk density (ρ_{bulk}), porosity (ε) and pore volume (V_p) of the dry HA materials.

Entry	Label	ρ_{bulk} (g/cm^3)	ε (%)	V_p (cm^3/g)
1	HA-E-0.5-1.5	0.057	96	16.83
2	HA-E-0.5-2.5	0.082	94	11.45
4	HA-E-0.5-12	0.270	79	2.93
5	HA-E-1.6-1.5	0.065	95	14.61
6	HA-E-1.6-2.5	0.150	88	5.91
8	HA-E-1.6-12	0.722	44	0.61
9	HA-A-0.5-1.5	0.141	90	6.34
10	HA-A-0.5-2.5	0.112	92	8.18
12	HA-A-0.5-12	0.574	59	1.02
13	HA-A-1.6-1.5	0.226	84	3.71
14	HA-A-1.6-2.5	0.247	82	3.33
15	HA-A-1.6-6.0	0.081	94	11.66
16	HA-A-1.6-12	0.952	31	0.33

3.4. Specific surface area and network morphology by SEM

Figure 5 shows the specific surface area values of all samples studied. Materials that were prepared at pH 6 or 12 in both ethanol and acetone and at pH 1.5 in acetone have a very low surface area, with some values close to the detection limit of the equipment. All these materials cannot be called "aerogels". We assume that at pH 12, the low surface area obtained with both non-solvents is most probably due to the degradation of HA at such high pH because of the cleavage of glycosidic bonds.[44] Indeed, the HA molecular weight in the HA-A-1.6-12 sample was found to be around $1 \cdot 10^5$ g/mol, which is only ~8 % of the molecular weight of the starting HA. Also, at this pH no hydrogen bonds (and thus no network) are formed as HA is totally deprotonated.[45] Short polymer chains are precipitating and collapsing forming a rather dense material (Figure 4) with rather low porosity and pore volume (Table 2), which are confirmed by SEM images (Figure 6a). At pH 6 it was possible to obtain only one self-standing precursor, for HA of 1.6% coagulated in acetone; the dry material was very fragile and difficult to handle, with low density (Figure 4) and low surface area (Figure 5). At this pH the polymer is still deprotonated and hardly forms a network. At pH 1.5 a material with low surface area was obtained when HA was coagulated in acetone (Figure 5). At this pH the carboxyl groups of HA are protonated allowing hydrogen bonds to be formed. However, the HA molecular weight in the HA-E-1.6-1.5 sample was found to be only 5500 g/mol, demonstrating that severe HA degradation takes place at this pH. Our finding is in line with previous research[44] reporting HA degradation at pH < 2 and implies that even if a weak network is formed, it will be composed of macromolecules of a decreased molecular weight. As mentioned above, HA has better affinity for ethanol than for acetone; we speculate that "harsh" coagulation in an aprotic non-solvent, acetone, leads to chain self-aggregation (Figure 6b) resulting in a dry network with low density (Figure 4) and low surface area (Figure 5).

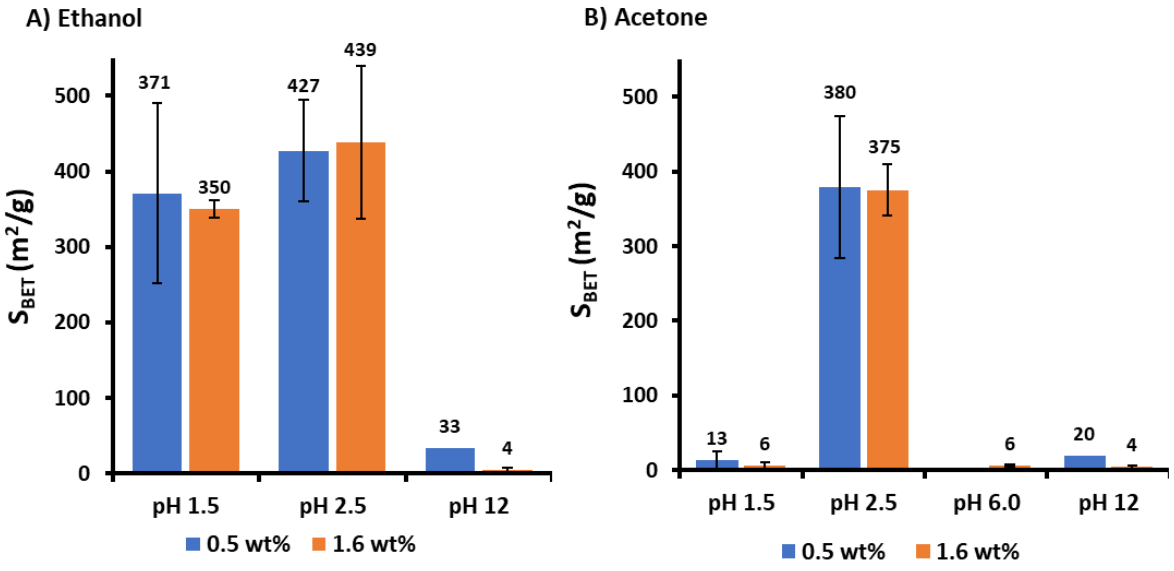

Figure 5

Specific surface area of HA dry materials obtained by coagulating in ethanol (A) and in acetone (B).

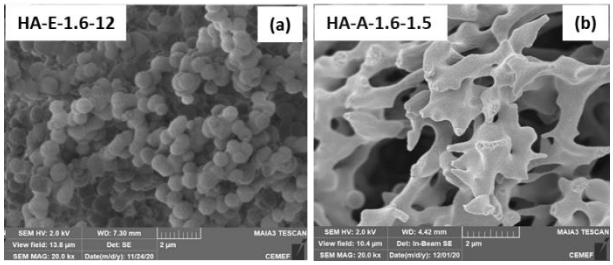

Figure 6

Examples of network morphology observed by SEM of samples HA-E-1.6-12 (a) and HA-A-1.6-1.5 (b).

According to the results obtained on specific surface area, aerogels, i.e. materials of low density and high surface area, were obtained from three types of formulations (for both concentrations of HA): at pH 1.5 when coagulated in ethanol and at pH 2.5 when coagulated in ethanol or in acetone (Figure 7). At pH 2.5 HA is at its isoelectric point forming a viscoelastic gel-like substance.[45] The

addition of a non-solvent leads to overall shrinkage but not to total collapse. A similar behavior was reported for pectin aerogels.[30] The highest surface area values, 470 – 510 m^2/g, were obtained when using ethanol coagulation which implies milder conditions in comparison with coagulation in acetone (see the solubility parameters in Table S1). The surface area of aerogels made from solutions at pH 1.5 coagulated in ethanol and at pH 2.5 coagulated in acetone is within the same range, 350 – 450 m^2/g. Overall, specific surface area (Figure 5) and morphology (Figures 6 and 7) demonstrate a striking difference between the materials obtained at pH 1.5 or 12 (collapsed network with thick pore walls formed of aggregated HA chains) and at pH 2.5 (aerogels: a network of fine fibrils with meso- and small macropores).

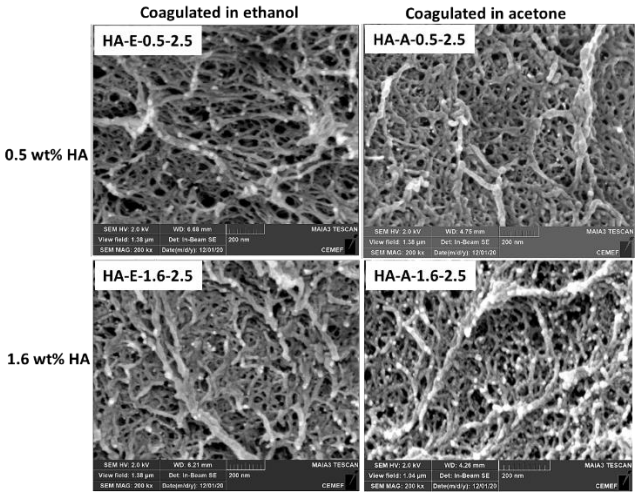

Figure 7

Examples of network morphology observed by SEM for the samples obtained from HA solutions at pH 2.5 and coagulated in ethanol or in acetone.

The pore size distribution of the four aerogels prepared at pH 2.5 was evaluated by image analysis as described in Methods section and as shown in Figure S3. Pore sizes are within 100 nm

with a median value around 15-17 nm not depending on polymer concentration or non-solvent used. This interval of mesopores and small macropores confirms HA aerogels' high specific surface area.

4. Conclusions

The feasibility of making non-crosslinked hyaluronic acid aerogels without any added compound was explored. Direct non-solvent induced phase separation was used as an approach to obtain HA self-standing 3D networks. Starting with 16 HA formulations, which differ in polymer concentration and pH of the solution as well as the type of non-solvent, it was possible to obtain 6 HA aerogels, all from low pH, either 1.5 or 2.5: three from 0.5 wt% (HA-E-0.5-1.5, HA-E-0.5-2.5 and HA-A-0.5-2.5) and three from 2.5 wt% (HA-E-1.6-1.5, HA-E-1.6-2.5 and HA-A-1.6-2.5) displaying high surface areas (up to 510 m^2/g) and low densities (values as low as 0.057 g/cm^3). The pH had a pronounced effect on the properties of the HA dry materials with pH 2.5, the HA isoelectric point, being the value that allowed for the formation of aerogels at all the conditions assessed. In contrast, the use of pH 12 led to non-porous dry materials with high densities, likely due to HA degradation, as demonstrated by the strong decrease of the HA molecular weight, and the absence of network formation in the precursors. At more acidic pH (1.5), despite a strong HA molecular weight decrease, the materials were sensitive to the type of the non-solvent whereby the use of ethanol allowed for the formation of aerogels. The results indicate that the degree of protonation of HA as well as its molecular weight play an important role in determining the stability of the precursor HA network and, as a consequence, the possibility of aerogel formation.

The type of the non-solvent had a major effect on the volume shrinkage and density with ethanol, a polar solvent, generating the least volume shrinkage and hence the lightest materials.

However, in comparison with acetone, more irregular shapes were obtained at the macroscopic level. The concentration only had a mild effect on the density revealing, in most of the cases, a proportional increment with polymer concentration. SEM images of the aerogels confirmed the formation of mesoporous materials at pH 2.5. The results validate our hypothesis that HA is a suitable polymer for the preparation of aerogels with appealing properties provided the preparation conditions are carefully selected. Overall, these novel HA aerogels display interesting textural and morphological properties with potential to be applied in the field of biomedical materials.

Acknowledgments

This work was carried out in the frame of the OLIBLOCK project of the French National Research Agency (ANR) and partly within the COST Action CA18125 "Advanced Engineering and Research of aeroGels for Environment and Life Sciences" (AERoGELS) funded by the European Commission. We would like to thank to Pierre Ilbizian (PERSEE, Mines Paris) for sc CO_2 drying and Suzanne Jacomet (CEMEF, Mines Paris) for SEM imaging. The measurement of the skeletal density was performed at the Department of Pharmacology of the University of Santiago de Compostela (Spain) for which we warmly acknowledge Dr. Carlos A. García-González.

Supporting Information: photos of HA samples, photos of sample volume evolution, table with solubility parameters and illustrations of pore size distribution analysis.

References

1. Budtova, T.; Aguilera, D. A.; Beluns, S.; Berglund, L.; Chartier, C.; Espinosa, E.; Gaidukovs, S.; Klimek-Kopyra, A.; Kmita, A.; Lachowicz, D.; Liebner, F.; Platnieks, O.; Rodríguez, A.; Tinoco Navarro, L. K.; Zou, F.; Buwalda, S. J. Biorefinery approach for aerogels. *Polymers* **2020**, *12*, 2779.

2. Zhao, S.; Malfait, W. J.; Guerrero-Alburquerque, N.; Koebel, M. M.; Nyström, G. Biopolymer aerogels and foams: Chemistry, properties, and applications. *Angew. Chem., Int. Ed.* **2018**, *57*, 7580-7608.

3. Muhammad, A.; Lee, D.; Shin, Y.; Park, J. Recent progress in polysaccharide aerogels: Their synthesis, application, and future outlook. *Polymers* **2021**, *13*, 1347.

4. Buwalda, S. J. Bio-based composite hydrogels for biomedical applications. *Multifunct. Mater.* **2020**, *3*, 022001.

5. Forgács, A.; Papp, V.; Paul, G.; Marchese, L.; Len, A.; Dudás, Z.; Fábián, I.; Gurikov, P.; Kalmár, J. Mechanism of hydration and hydration induced structural changes of calcium alginate aerogel. *ACS Appl. Mater. Interfaces* **2021**, *13*, 2997-3010.

6. Zou, F.; Budtova, T. Tailoring the morphology and properties of starch aerogels and cryogels via starch source and process parameter. *Carbohydr. Polym.* **2021**, *255*, 117344.

7. Druel, L.; Niemeyer, P.; Milow, B.; Budtova, T. Rheology of cellulose-[DBNH][CO 2 Et] solutions and shaping into aerogel beads. *Green Chem.* **2018**, *20*, 3993-4002.

8. Preibisch, I.; Niemeyer, P.; Yusufoglu, Y.; Gurikov, P.; Milow, B.; Smirnova, I. Polysaccharide-based aerogel bead production via jet cutting method. *Materials* **2018**, *11*, 1287.

9. Druel, L.; Kenkel, A.; Baudron, V.; Buwalda, S. J.; Budtova, T. Cellulose aerogel microparticles via emulsion-coagulation technique. *Biomacromolecules* **2020**, *21*, 1824-1831.

10. Obaidat, R. M.; Alnaief, M.; Mashaqbeh, H. Investigation of carrageenan aerogel microparticles as a potential drug carrier. *AAPS PharmSciTech* **2018**, *19*, 2226-2236.

11. Zou, F.; Budtova, T. Polysaccharide-based aerogels for thermal insulation and superinsulation: An overview. *Carbohydr. Polym.* **2021**, *266*, 118130.

12. Selvasekaran, P.; Chidambaram, R. Food-grade aerogels obtained from polysaccharides, proteins, and seed mucilages: Role as a carrier matrix of functional food ingredients. *Trends Food Sci. Technol.* **2021**, *112*, 455-470.

13. Kobina Sam, D.; Kobina Sam, E.; Lv, X. Application of biomass-derived nitrogen-doped carbon aerogels in electrocatalysis and supercapacitors. *ChemElectroChem* **2020**, *7*, 3695-3712.

14. Maleki, H. Recent advances in aerogels for environmental remediation applications: A review. *Chem. Eng. J.* **2016**, *300*, 98-118.

15. Maleki, H.; Durães, L.; García-González, C. A.; del Gaudio, P.; Portugal, A.; Mahmoudi, M. Synthesis and biomedical applications of aerogels: Possibilities and challenges. *Adv. Colloid Interface Sci.* **2016**, *236*, 1-27.

16. García-González, C. A.; Budtova, T.; Durães, L.; Erkey, C.; Del Gaudio, P.; Gurikov, P.; Koebel, M.; Liebner, F.; Neagu, M.; Smirnova, I. An opinion paper on aerogels for biomedical and environmental applications. *Molecules* **2019**, *24*, 1815.

17. Groult, S.; Buwalda, S.; Budtova, T. Pectin hydrogels, aerogels, cryogels and xerogels: Influence of drying on structural and release properties. *Eur. Polym. J.* **2021**, *149*, 110386.

18. Groult, S.; Buwalda, S.; Budtova, T. Tuning bio-aerogel properties for controlling theophylline delivery. Part 1: Pectin aerogels. *Mater. Sci. Eng., C* **2021**, *126*, 112148.

19. Groult, S.; Buwalda, S.; Budtova, T. Tuning bio-aerogel properties for controlling drug delivery. Part 2: Cellulose-pectin composite aerogels. *Biomaterials Advances* **2022**, in press, https://doi.org/10.1016/j.bioadv.2022.212732

20. Mihajlovic, M.; Fermin, L.; Ito, K.; van Nostrum, C. F.; Vermonden, T. Hyaluronic acid-based supramolecular hydrogels for biomedical applications. *Multifunct. Mater.* **2021**, *4*, 032001.

21. Collins, M. N.; Birkinshaw, C. Hyaluronic acid based scaffolds for tissue engineering - A review. *Carbohydr. Polym.* **2013**, *92*, 1262-1279.

22. Alven, S.; Aderibigbe, B. A. Hyaluronic acid-based scaffolds as potential bioactive wound dressings. *Polymers* **2021**, *13*, 2102.

23. Poldervaart, M. T.; Goversen, B.; de Ruijter, M.; Abbadessa, A.; Melchels, F. P. W.; Oner, F. C.; Dhert, W. J. A.; Vermonden, T.; Alblas, J. 3D bioprinting of methacrylated hyaluronic acid (MeHA) hydrogel with intrinsic osteogenicity. *PLoS One* **2017**, *12*, e0177628.

24. Tavsanli, B.; Okay, O. Macroporous methacrylated hyaluronic acid cryogels of high mechanical strength and flow-dependent viscoelasticity. *Carbohydr. Polym.* **2020**, *229*, 115458.

25. Bucatariu, S.; Constantin, M.; Varganici, C.; Rusu, D.; Nicolescu, A.; Prisacaru, I.; Carnuta, M.; Anghelache, M.; Calin, M.; Ascenzi, P. A new sponge-type hydrogel based on hyaluronic acid and poly (methylvinylether-alt-maleic acid) as a 3D platform for tumor cell growth. *Int. J. Biol. Macromol.* **2020**, *165*, 2528-2540.

26. Zamboni, F.; Okoroafor, C.; Ryan, M. P.; Pembroke, J. T.; Strozyk, M.; Culebras, M.; Collins, M. N. On the bacteriostatic activity of hyaluronic acid composite films. *Carbohydr. Polym.* **2021**, *260*, 117803.

27. Highley, C. B.; Prestwich, G. D.; Burdick, J. A. Recent advances in hyaluronic acid hydrogels for biomedical applications. *Curr. Opin. Biotechnol.* **2016**, *40*, 35-40.

28. Athamneh, T.; Amin, A.; Benke, E.; Ambrus, R.; Leopold, C. S.; Gurikov, P.; Smirnova, I. Alginate and hybrid alginate-hyaluronic acid aerogel microspheres as potential carrier for pulmonary drug delivery. *J. Supercrit. Fluids* **2019**, *150*, 49-55.

29. Athamneh, T.; Amin, A.; Benke, E.; Ambrus, R.; Gurikov, P.; Smirnova, I.; Leopold, C. S. Pulmonary drug delivery with aerogels: engineering of alginate and alginate–hyaluronic acid microspheres. *Pharm. Dev. Technol.* **2021**, *26*, 509-521.

30. Groult, S.; Budtova, T. Tuning structure and properties of pectin aerogels. *Eur. Polym. J.* **2018**, *108*, 250-261.

31. Buchtova, N.; Budtova, T. Cellulose aero-, cryo-and xerogels: towards understanding of morphology control. *Cellulose* **2016**, *23*, 2585-2595.

32. Rudaz, C.; Courson, R.; Bonnet, L.; Calas-Etienne, S.; Sallee, H.; Budtova, T. Aeropectin: fully biomass-based mechanically strong and thermal superinsulating aerogel. *Biomacromolecules* **2014**, *15*, 2188-2195.

33. Aegerter, M. A.; Leventis, N.; Koebel, M. M. *Aerogels handbook;* Springer Science & Business Media, 2011.

34. García-Abuín, A.; Gómez-Díaz, D.; Navaza, J. M.; Regueiro, L.; Vidal-Tato, I. Viscosimetric behaviour of hyaluronic acid in different aqueous solutions. *Carbohydr. Polym.* **2011**, *85*, 500-505.

35. Hansen, C.M., *Hansen Solubility Parameters: A User's Handbook*, 2nd ed. CRC Press, Boca Raton. **2007**

36. Shi, C.; Sun, Y.; Wu, H.; Zhu, C.; Wei, G.; Li, J.; Chan, T.; Ouyang, D.; Mao, S. Exploring the effect of hydrophilic and hydrophobic structure of grafted polymeric micelles on drug loading. *Int. J. Pharm.* **2016,** *512*, 282-291

37. Innerlohinger, J.; Weber, H. K.; Kraft, G. Aerocellulose: aerogels and aerogel-like materials made from cellulose. *Macromol. Symp.* **2006**, *244*, 126-135.

38. Robitzer, M.; Di Renzo, F.; Quignard, F. Natural materials with high surface area. Physisorption methods for the characterization of the texture and surface of polysaccharide aerogels. *Microporous Mesoporous Mater.* **2011**, *140*, 9-16.

39. Gavillon, R.; Budtova, T. Kinetics of cellulose regeneration from cellulose−NaOH−water gels and comparison with cellulose−N-methylmorpholine-N-oxide−water solutions. *Biomacromolecules* **2007**, *8*, 424-432.

40. Schestakow, M.; Karadagli, I.; Ratke, L. Cellulose aerogels prepared from an aqueous zinc chloride salt hydrate melt. *Carbohydr. Polym.* **2016**, *137*, 642-649.

41. Manzocco, L.; Valoppi, F.; Calligaris, S.; Andreatta, F.; Spilimbergo, S.; Nicoli, M. C. Exploitation of κ-carrageenan aerogels as template for edible oleogel preparation. *Food Hydrocoll.* **2017**, *71*, 68-75.

42. Guerrero-Alburquerque, N.; Zhao, S.; Adilien, N.; Koebel, M. M.; Lattuada, M.; Malfait, W. J. Strong, machinable, and insulating chitosan–urea aerogels: Toward ambient pressure drying of biopolymer aerogel monoliths. *ACS Appl. Mater. Interfaces* **2020**, *12*, 22037-22049.

43. Buchtová, N.; Pradille, C.; Bouvard, J.; Budtova, T. Mechanical properties of cellulose aerogels and cryogels. *Soft Matter* **2019**, *15*, 7901-7908.

44. Maleki, A.; Kjøniksen, A.; Nyström, B. Effect of pH on the behavior of hyaluronic acid in dilute and semidilute aqueous solutions. *Macromol. Symp.* **2008**, *274*, 131-140.

45. Gatej, I.; Popa, M.; Rinaudo, M. Role of the pH on hyaluronan behavior in aqueous solution. *Biomacromolecules* **2005**, *6*, 61-67.

Graphic for the Table of Content

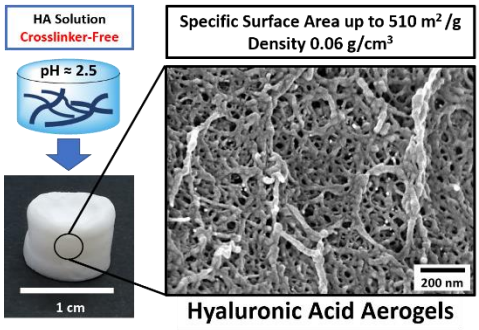

Supporting Information

Crosslinker-free hyaluronic acid aerogels

Daniel Aguilera-Bulla, Laurianne Legay, Sytze J. Buwalda*, Tatiana Budtova*

MINES Paris, PSL Research University, Center for Materials Forming (CEMEF), UMR CNRS 7635, CS 10207, 06904 Sophia Antipolis, France.

Corresponding authors:

Tatiana.Budtova@minesparis.psl.eu

Sijtze.Buwalda@minesparis.psl.eu

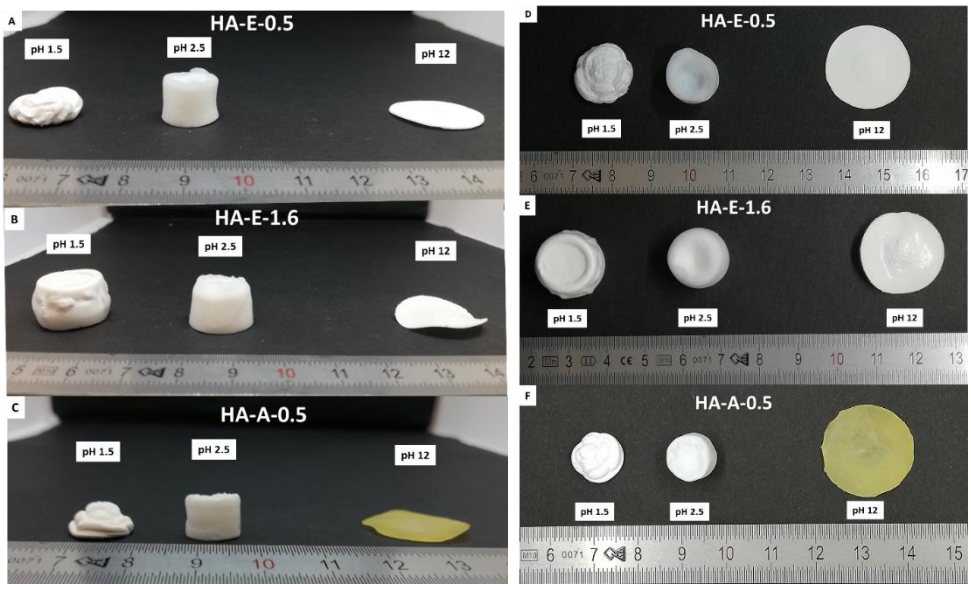

Figure S1

Side (A, B, C) and top (D, E, F) views of dry HA materials.

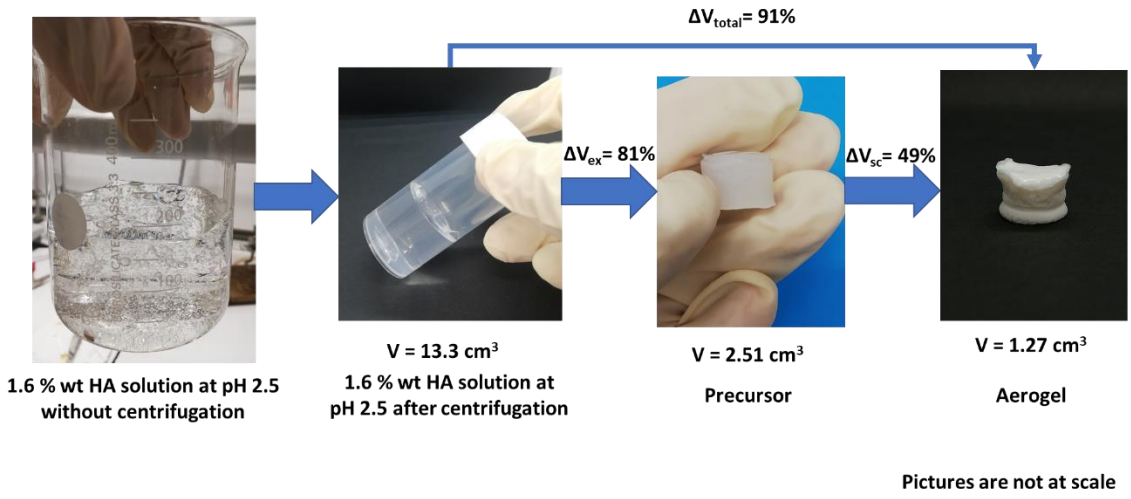

Figure S2

Example of sample volume evolution for 1.6 wt% HA solution at pH 2.5, acetone was used as non-solvent.

Table S1. Dispersion (δ_d), polar (δ_p), hydrogen bonding (δ_h) and total (δ) solubility parameters for HA, ethanol and acetone.

Compound	δ_d (MPa$^{1/2}$)	δ_p (MPa$^{1/2}$)	δ_h (MPa$^{1/2}$)	δ (MPa$^{1/2}$)
HA[a]	28.2	11.2	18.9	35.8
Ethanol[b]	15.8	8.8	19.4	26.5
Acetone[b]	15.5	10.4	7.0	19.9

[a] Solubility parameters δ_d, δ_p, δ_h and taken from reference [1], δ is calculated according to eq.2.

[b] Solubility parameters taken from reference [2].

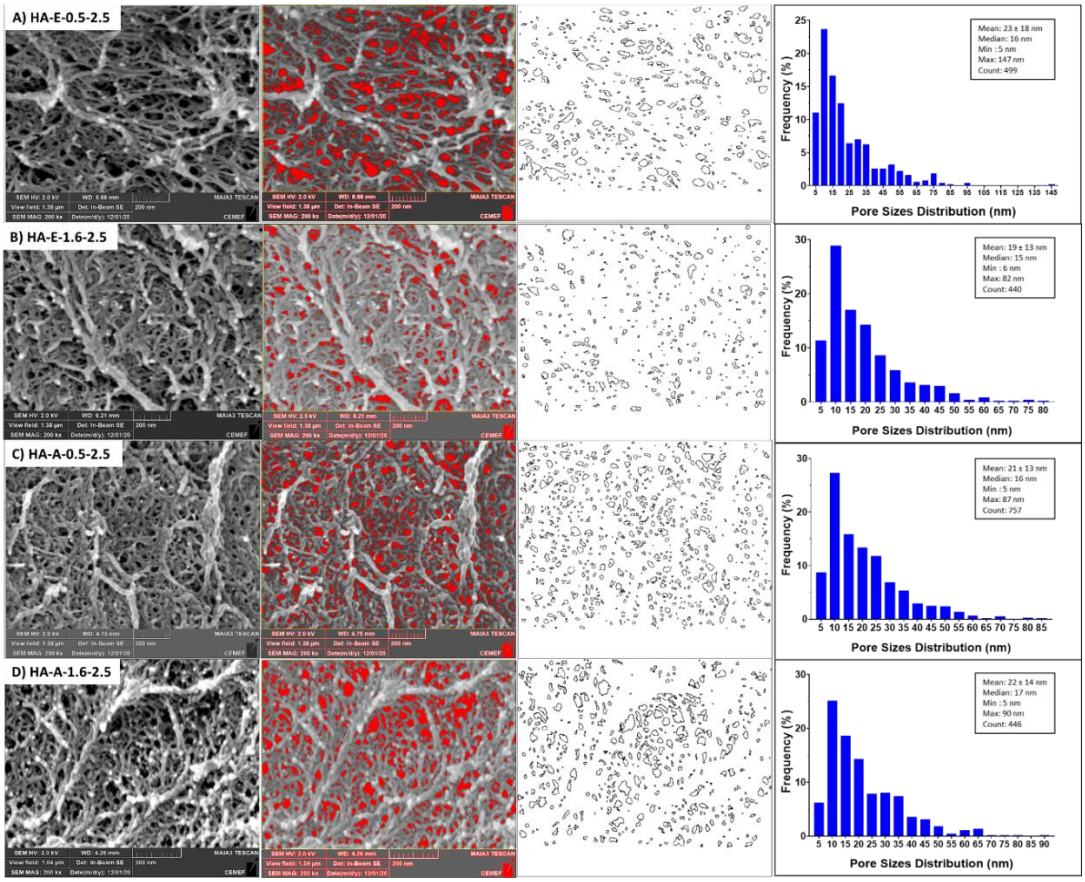

Figure S2

Examples of image analysis steps for the determination of pore size distribution for the simples A) HA-E-0.5-2.5, B) HA-E-1.6-2.5, C) HA-A-0.5-2.5 and D) HA-A-1.6-2.5. From left to right:

SEM image of aerogel; threshold adjustment to detect pores (in red); map of the pores calculated by ImageJ and pore size distribution.

References

1. Shi, C.; Sun, Y.; Wu, H.; Zhu, C.; Wei, G.; Li, J.; Chan, T.; Ouyang, D.; Mao, S. Exploring the effect of hydrophilic and hydrophobic structure of grafted polymeric micelles on drug loading. *Int. J. Pharm.* **2016,** *512*, 282-291.
2. Hansen, C.M., *Hansen Solubility Parameters: A User's Handbook*, 2nd ed. CRC Press, Boca Raton. **2007**